RESEARCH ARTICLE

Water Entry Problems Simulated by an Axisymmetric SPH Model with VAS Scheme

Xiaoting Huang[1,2], Pengnan Sun[1,2], Hongguan Lyu[1,2] and A-Man Zhang[3]

Abstract

Water entry of marine structures has long been an important problem in ocean engineering. Among the different techniques to predict fluid-structure interactions during water entry, smoothed particle hydrodynamics (SPH) method gradually becomes a promising method that is able to solve the impact pressure and the splashing fluid jets simultaneously. However, for three-dimensional (3D) problems, SPH method is computationally expensive due to the huge number of particles that are needed to resolve the local impact pressure accurately. Therefore, in this work an axisymmetric SPH model is applied to solve different water entry problems with axisymmetric structures including spheres and cones with different deadrise angles. Importantly, the Volume Adaptive Scheme (VAS) is added to guarantee the homogeneousness of particle volumes during the simulation. The axisymmetric SPH model with VAS scheme will be introduced in detail and the numerical results will be sufficiently validated with experimental data to demonstrate the high robustness and accuracy of the SPH model for solving 3D axisymmetric water entry problems in an efficient way.

1 Introduction

Water entry of structures, as a fundamental and widely concerned mechanical issue, is tightly related to many applications in engineering. In particular, water entry problems are frequently encountered in ocean engineering applications, e.g. free-fall of lifeboats (Huang et al., 2021), launching of torpedoes from air, aircraft ditching (Woodgate et al., 2019; Xiao et al., 2017), ship slamming (Cheng et al., 2020), etc. To ensure safety of marine vehicles, the physical characteristics of the marine structure after water entry should be well studied and understood, including the velocity and acceleration variation of the structure, the pressure loaded on the structure surface and the fluid splashing induced by the strong impact (Lin, 2007).

The first significant study of water entry was conducted by Von Karman and Wattendorf (1929) who estimated the slamming forces on wedges according to conservation of fluid-wedge momentum theory and the added mass effect, which was applied to predict the maximal pressure estimation on the floats of hydroplanes during sea landings. Wagner (1932) also investigated a similar issue for the impact of objects on liquid surfaces. Later, based on the velocity potential theories, Dobrovol'skaya (1969) investigated a two-dimensional wedge water entry problem. However, in these theories, the water entry models were limited to ideal conditions so that it is not enough to reflect the real water entry process of marine structures with complex shapes considering the effects of air phase and fluid compressibility.

Article Highlights

- The axisymmetric-SPH model with VAS scheme is extended to investigating water entry problems.
- 3D problems can be simulated in a 2D plane with good accuracy and lower computational cost.
- With refined particle resolutions, the local impact pressure on the body surface is predicted well.
- Motion characteristics of the rigid body agree well with experimental data and other numerical solutions.

✉ Pengnan Sun
   sunpn@mail.sysu.edu.cn

[1] School of Ocean Engineering and Technology, Sun Yat-sen University, Zhuhai 519082, China.

[2] Southern Marine Science and Engineering Guangdong Laboratory (Zhuhai), Zhuhai 519082, China.

[3] College of Shipbuilding Engineering, Harbin Engineering University, Harbin 150001, China.

After that, numerous experimental studies were reported on the water entry of the various axisymmetric shapes. For example, the experiment by Moghisi and Squire (1981) reported the initial impact force on a sphere striking a liquid surface. The study of Lin and Shieh (1997) provided experimental data for impact pressure and the acceleration of structures with circular cylindrical shapes. Yettou et al. (2006) investigated the pressure distribution on a free-falling wedge upon entering water experimentally. Especially, Truscott and Techet (2009) investigated experimentally the water entry of both spinning and non-spinning spheres at low Froude numbers. In particular, Aristoff et al. (2010) combined experimental and theoretical methods to predict the sphere dynamics. Indeed, the experimental tests provide plenty of reliable results to conclude the mechanism of water entry problems. However, due to the limitations of expensive cost and long experimental duration, the experimental method is not efficient, convenient and simple to investigate the water entry issues. To foster the research on alternative methods, more computational fluid dynamics (CFD) solvers are developed which can avoid the high expense in experiments and simulate more complex conditions compared to analytical models (Zhao and Faltinsen, 1993; Yu et al., 2015). Using the Eulerian mesh-based solvers, Iranmanesh and Passandideh-Fard (2017) investigated the water entry of a horizontal circular cylinder in three dimensions (3D), tracking the free surface using the VOF method. In addition, detailed studies on water entry problems were carried by Van Nuffel et al. (2014); Wang and Soares (2020); Wang et al. (2021); Wang and Soares (2022). As mentioned before, the treatment of free surface is complicated for grid-based Eulerian methods. Further, the sharpness of free surfaces could be lost in the space where the mesh resolution is not fine enough. In contrast, the mesh-free method or particle method owns significant advantages for such problems with splashing free surface.

Smoothed particle hydrodynamics (SPH) method, thanks to its Langrangian feature, is capable of dealing with the free surface breaking and water splashing (Yang et al., 2020), demonstrating that the SPH is a competitive method for ocean engineering applications, see Ye et al. (2019); Liu and Zhang (2019); He et al. (2020); Long et al. (2021); Luo et al. (2021); Sun et al. (2021a); and Lyu et al. (2022a). Actually, extensive SPH simulations were accomplished for the water entry problems, see Shao (2009); Skillen et al. (2013a); Khayyer and Gotoh (2016); Gong et al. (2016); Zhang et al. (2017); Sun et al. (2018); and Wang et al. (2019). The authors simulated the water entry of rigid bodies including wedge, sphere and plate using weakly-compressible (see e. g. Oger et al. (2006); Vandamme et al. (2011); and Omidvar et al. (2012)) or incompressible SPH models (Shao and Gotoh, 2004; Bøckmann et al., 2012; and Skillen et al., 2013b). However, most of the SPH simulations are limited to two dimensions (2D). Further, most

investigations were performed with single-phase SPH model, neglecting the effect of air. For some fluid impact problems, the air phase has a significant influence on the flow evolution and the slamming load on structures. To simulate multiphase flows, SPH has been proved to be an excellent method (Colagrossi and Landrini, 2003; Hammani et al., 2020) thanks to its advantage of tracking the particles in a Lagrangian fashion, and therefore, the interface between two phases can be straightforwardly captured. In that way, the water entry process can be simulated accurately.

Importantly, as highlighted in Marrone et al. (2017), the water entry simulation using SPH in 3D would lead to enormous computational cost, so that it is challenging for engineering applications. From this aspect, for some axisymmetric problems, SPH simulation in the cylindrical coordinate system can be applied to save the computational cost. Ming et al. (2014) adopted an axisymmetric SPH model to study underwater explosion problems. Brookshaw (2003) proposed an axisymmetric SPH discretization in the cylindrical coordinate, while their model has an obstacle to treating with the axis singularity. Recently, Gong et al. (2019) developed an axisymmetric SPH model under the weakly-compressible assumption for water entry problems. For the above-mentioned axisymmetric SPH studies, the treatment of the symmetric axis is not easy due to the singularity which could lead to problems of numerical instability. Recently, Sun et al. (2021b) adopted the ghost particles mirrored on the other side of the axis, avoiding axis singularities and, further, they proposed a Volume Adaptive Scheme (VAS) to keep uniform particle distributions with homogeneous volumes. Later, Fang et al. (2022) extended this technique to the framework of Riemann-SPH, and investigated different multiphase flows with complex interfaces. In the above studies, the axisymmetric SPH model has been applied to water entry problems, but in their works the axisymmetric SPH simulations were mainly applied to predict the motions of the structure, without carefully validating the local impact pressure which will be carried out in the present work. In addition, the particle resolution was not fine enough in previous studies and therefore the splashing jets were not captured accurately.

In the present work, an axisymmetric SPH method is implemented for different water entry problems with different structures, including sphere and cones with different deadrise angles. Similar to Sun et al. (2021b), the VAS is applied to ensure the homogeneousness of the particle volumes. To investigate the water entry problems more comprehensively, the local impact pressure will be carefully validated and discussed after a convergence study. In addition, the slashing jets are captured and carefully compared with experimental snapshots.

The paper is arranged as follows: Section 2 introduces the axisymmetric SPH model, the treatment of singularity

at axis, the volume adaptive scheme and the boundary conditions. Section 3 displays results of water entry simulations validated with experiment data, demonstrating the accuracy and advantages of the axisymmetric SPH model after convergence analysis. Finally, Section 4 gives concluding remarks and perspectives regarding the SPH simulation of water entry in the present work and in the future studies.

2 Axisymmetric SPH model

2.1 Governing equations and axisymmetric simplification

To simulate the water entry problems, similar to the previous studies (Lyu et al., 2021; Gong et al., 2016), the fluid is assumed to be inviscid and weakly-compressible. Grounded on these assumptions, the governing equations in cylindrical coordinates (Gong et al., 2019) are presented as follows:

$$\begin{cases} \dfrac{D\rho}{Dt} = -\dfrac{\rho}{r}\left[\dfrac{\partial}{\partial r}(rv^r) + \dfrac{\partial v^\theta}{\partial \theta} + r\dfrac{\partial v^z}{\partial z} \right], \\[2mm] \dfrac{Dv^r}{Dt} = -\dfrac{1}{\rho}\dfrac{\partial p}{\partial r}, \\[2mm] \dfrac{Dv^\theta}{Dt} = -\dfrac{1}{\rho r}\dfrac{\partial p}{\partial \theta}, \\[2mm] \dfrac{Dv^z}{Dt} = -\dfrac{1}{\rho}\dfrac{\partial p}{\partial z} - g^z, \end{cases} \quad (1)$$

in which ρ and p represent density and pressure, respectively. The v^r, v^θ and v^z denote the three components of the velocity vector v in the radial(r), circumferential (θ) and axial (z) directions, respectively. g^z is the magnitude of the gravity acceleration in the z direction. The first equation in Eq. (1) represents the continuity equation and other three equations are the components of momentum equation described in three dimensional coordinates (r-θ-z).

Under the axisymmetric assumption, the circumferential velocity component $v^\theta=0$ and the partial derivative of pressure $\partial p/\partial \theta=0$ (Sun et al., 2021b). The governing equations in Eq. (1) can be simplified as follows:

$$\begin{cases} \dfrac{D\rho}{Dt} = -\rho\dfrac{v^r}{r} + \rho\left(\dfrac{\partial v^r}{\partial r} + \dfrac{\partial v^z}{\partial z} \right), \\[2mm] \dfrac{Dv^r}{Dt} = -\dfrac{1}{\rho}\dfrac{\partial p}{\partial r}, \\[2mm] \dfrac{Dv^z}{Dt} = -\dfrac{1}{\rho}\dfrac{\partial p}{\partial z} - g^z \end{cases} \quad (2)$$

Therefore, the water entry problems can be simplified by reducing the problem to an axisymmetric one, see Figure 1.
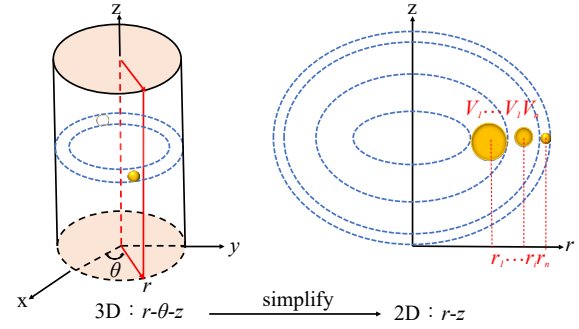

Figure 1 The diagram showing the simplification from a 3D cylindrical coordinates system to a 2D axisymmetric plane. In the 2D plane on the right side, the particle mass m_i is equal to the torus mass in the 3D cylindrical coordinate system, which should be conserved in the flow evolution unless a particle splitting or coalescing occurs. Therefore, the particle volume V_i varies directly when the radial coordinate r_i changes (Sun et al., 2019)

2.2 Discretizations

The water entry of axisymmetric body can be simulated using the axisymmetric SPH model with particles only distributed in r-z plane, thus straightforwardly avoiding the enormous number of fluid particles needed in the purely 3D SPH simulations. The governing equations (Eq. (2) (Sun et al., 2021b)) are discretized as

$$\begin{cases} \dfrac{D\rho_i}{Dt} = -\rho_i\dfrac{v_i^r}{r_i} - \rho_i < \nabla \cdot \boldsymbol{v} >_i^{L1} + \delta\sum_j \phi_{ij}c_{ij}h\mathbf{D}_{ij}\cdot\nabla_iW_{ij}V_j, \\[2mm] \dfrac{D\boldsymbol{v}_i}{Dt} = \dfrac{1}{\rho_i} < \nabla p >^{L2} + \boldsymbol{g}_i + \sum_j\dfrac{\rho_j}{\rho_{ij}}\pi_{ij}\nabla_iW_{ij}V_j, \\[2mm] \dfrac{D\boldsymbol{r}_i}{Dt} = \boldsymbol{v}_i, \end{cases} \quad (3)$$

where the subscript i denotes the i-th particle and j denotes the particles in the kernel supporting region of i. v and g have components in two directions, denoted as $\boldsymbol{v} = (v^r, v^z)$ and $\boldsymbol{g}=(0,-g^z)$. ρ_{ij} is denoted as $(\rho_i + \rho_j)/2$. W_{ij} represents the kernel function for which the Wendlend C2 kernel is used in this work. The smoothing length is set to $h = 2\Delta x$ where Δx denotes the particle spacing. r_i is the vector of particle position of particle i. For the sake of stabilizing the density/pressure and velocity fields, the diffusive terms with D_{ij} and π_{ij} are added in governing equations(Antuono et al., 2010, 2012). The constant parameter $\delta = 0.1$ is used in the density diffusive term. D_{ij} is defined as follows:

$$\mathbf{D}_i = 2\sum_j \psi_{ji}\dfrac{(\boldsymbol{r}_j - \boldsymbol{r}_i)\cdot\nabla_iW_{ij}}{|\boldsymbol{r}_j - \boldsymbol{r}_i|^2}, \quad (4)$$

in which

$$\psi_{ji} = (\rho_j - \rho_i) - \dfrac{1}{2}(< \nabla\rho >_i^{L1} + < \nabla\rho >_j^{L1})\cdot(\boldsymbol{r}_j - \boldsymbol{r}_i), (5)$$

where $<\nabla\rho>_i^L$ and $<\nabla\rho>_j^L$ represent the renormalized density gradient (Randles and Libersky, 1996), and r_i represents the position vector of particle i. The viscous term π_{ij} is given as

$$\pi_{ij} = \alpha c_{ij} h \frac{(v_j - v_i)\cdot(r_j - r_i)}{|r_j - r_i|^2}, \tag{6}$$

where, to ensure numerical stability, the constant parameter $\alpha=0.05$ is used for water, $\alpha=0.3$ is used for air and $c_{ij}=(c_i + c_j)/2$. Further, to regularize the particle distribution, the particle shifting technique (PST) is adopted. More details can be seen in Sun et al. (2019, 2021b).

Finally, the velocity divergence $<\nabla\cdot v>^{L1}$, density gradient $<\nabla\rho>^{L1}$ and pressure gradient $<\nabla p_i>^{L2}$ are discretized similar to Sun et al. (2021b), written as

$$\begin{cases} <\nabla\cdot v>_i^{L1} := \sum_j (v_j - v_i)\cdot\nabla_i W_{ij}^C V_j \\ <\nabla\rho>_i^{L1} := \sum_j (\rho_j - \rho_i)\nabla_i W_{ij}^C V_j \\ <\nabla p>_i^{L2} := \sum_j (p_i \mathbf{L}_i + p_j \mathbf{L}_j)\nabla_i W_{ij} V_j, \\ \nabla_i W_{ij}^C := \mathbf{L}_i \nabla_i W_{ij}; \quad \mathbf{L}_i := \left[\sum_j (r_j - r_i)\otimes \nabla_i W_{ij} V_j\right]^{-1} \end{cases} \tag{7}$$

In addition, the technique of Tensile Instability Control is applied to reformulate the pressure gradient term to prevent the tensile instability when the pressure becomes negative, more details see Sun et al. (2017).

2.3 The equation of state

In order to obtain the pressure of fluid particles, the equation of state is applied to link the density and pressure (Colagrossi and Landrini, 2003), written as:

$$p = \frac{c_0^2 \rho_0}{\gamma}\left[\left(\frac{\rho}{\rho_0}\right)^\gamma - 1\right] + p_0 \tag{8}$$

where c_0 is the artificial sound speed and ρ_0 is the reference density when the particle pressure is equal to the background pressure p_0. For water entry problems, the air and water phase are both taken into consideration. The pressure for two phases is calculated with Eq. (8). In the multiphase SPH model, following Colagrossi and Landrini (2003), the polytrophic coefficient γ is set as $\gamma_w=7$ for water and $\gamma_a=1.4$ for air. To satisfy the weakly-compressible assumption, in the water phase, the density variation should be less than 1% of ρ_0, i.e. $\rho/\rho_0<1\%$. In order to meet this requirement, the artificial sound speed c_{0w} of water is constrained by the maximum expected pressure p_{max} and velocity v_{max} (Sun et al.,

2017), written as

$$c_{0w} \geqslant 10\max\left(v_{max}, \sqrt{\frac{p_{max}}{\rho_0}}\right) \tag{9}$$

As for the gas phase, the speed of sound c_{0a} (Sun et al., 2021) is given as

$$c_{0a} = \sqrt{\frac{c_{0w}^2 \rho_{0w}\gamma_a}{\rho_{0a}\gamma_w}} \tag{10}$$

In all the SPH simulations, the reference density of water is set as 1 000 kg/m^3 while the one of air is set as 1.29 kg/m^3. It leads to a larger sound speed in the air phase, reducing the time step and therefore making the computational cost of multiphase SPH simulations very expensive. But in this work, thanks to the axisymmetric SPH model, the 3D problem can be simulated in a 2D plane, therefore particle numbers are significantly reduced. In addition, the fourth-order-Runge-Kutta format is implemented to integrate the governing equations (Sun et al., 2021b). The time step is determined by:

$$\Delta t = \min\left(0.25 \min_i \sqrt{\frac{h_i}{|a_i|}}, CFL \min_i \frac{h_i}{c_0}\right) \tag{11}$$

where the sound speed c_0 is selected using the maximum value between c_{0a} and c_{0w}, and the CFL number is set as 0.5. Constrained by the above condition, the time step in simulations is small enough to keep stability. Recently, He et al. (2022) proposed a stable multiphase SPH model with a larger CFL number which could further improve the numerical efficiency.

2.4 Treatment of symmetry axis

In the present axisymmetric SPH scheme, the treatment of the symmetry axis is an essential but challenging problem. Firstly, the particles close to the axis ($r \to 0$) would lack neighbor particles in the domain of $r<0$, resulting in the truncated kernel support. Further, the calculation of $1/r_i$ in governing equations (Eq.(3)) at the axis, i.e. $r\to0$, would lead to numerical singularity. To solve this problem, on the other side of the axis (i.e. $r<0$) and within a distance of $2h$, ghost particles are created based on mirroring the fluid particles with respect to the axis. Noting that the velocity of ghost particles takes the same value of the fluid velocity in the z-direction, but takes the opposite value in the r-direction. The other physical quantities of ghost particle are directly copied from the corresponding fluid particles (Sun et al., 2021b). Finally, quantities of the ghost particles are given as

$$\begin{cases} m_g = m_f, \quad h_g = h_f, \\ v_g^r = -v_f^{\,r}, \quad v_g^z = v_f^z, \\ p_g = p_f, \quad \rho_g = \rho_f, \end{cases} \qquad (12)$$

where the subscript g and f represent the ghost particles and fluid particles, respectively. In fact, the calculation of SPH divergence and gradient operators in Eq. (7) is not affected by the term $1/r$. Further, with the ghost particles, the fluid particles are bounced back when they are about to penetrate the axis. Therefore, the singularity at the axis can be naturally avoided, guaranteeing the numerical stability.

2.5 Volume adaptive scheme (VAS)

Thanks to the Lagrangian properties of SPH model and especially in the axisymmetric SPH model, each fluid particle represents a fluid torus in the 3D space. When simplifying from 3D space to the 2D r-z plane, as shown in Figure 1, each particle volume in 2D represents the cross-section of the fluid torus (Sun et al., 2021b), written as

$$V_i(t) = \frac{m_i}{2\pi r_i(t)\rho_i(t)}, \qquad (13)$$

which indicates that the particle volume varies with the distance to the axis $r_i(t)$. Therefore, to limit the range of the volume variation, the VAS proposed by Sun et al. (2021,b) is implemented in the current work.

Limitation of the volume variation is realized with particle splitting and merging. Particle splitting is triggered when its volume is too large, while particle merging is triggered when its volume is too small, which aims to avoid clustered or sparse particle distributions. The process of VAS is shown in Figure 2. The step of splitting or merging is determined by the ratio between the real-time particle volume and the reference one. Specifically, if the particle volume V exceeds V_{max} (restriction on particle growing), the mother particle will be split into four daughter particles distributed on the vertices of a square (Sun et al., 2021b), assigned with the particle volume of $V_{max}/4$. As aforementioned, the VAS scheme is designed to homogenize particle distribution, guaranteeing the volume variation in a small range. That means the volume variation before splitting is equal to the volume variation after splitting (Sun et al., 2021), i.e. satisfying the following relation:

$$\| V_{max} - V_0 \| = \left(V_0 - \frac{V_{max}}{4} \right), \qquad (14)$$

where $V_{max}=1.6\,V_0$ is obtained from Eq.(14). Accordingly, after splitting, the minimum particle volume of daughter particles is $0.4\,V_0$, and the maximum volume variation for all particles remains less than $0.6V_0$. Other field quantities of the daughter particles can be obtained via the following criteria (Sun et al., 2021) as

$$\begin{cases} \boldsymbol{r}_d = \boldsymbol{r}_m \pm \frac{\sqrt{V_m}}{4}, \quad z_d = z_m \pm \frac{\sqrt{V_m}}{4}, \\ m_d = \frac{2\pi\rho_m V_m}{4} r_d, \quad V_d = \frac{m_d}{2\pi r_d \rho_d}, \quad h_d = h_m, \\ p_d = p_m + <\nabla p>_m \cdot (\boldsymbol{r}_d - \boldsymbol{r}_m), \quad \rho_d = F_{state}^{-1}(p_d), \quad \boldsymbol{v}_d = \boldsymbol{v}_m, \end{cases} \qquad (15)$$

where the subscript d and m denote the daughter particles and mother particles, respectively.

As shown in Figure 2, the particle merging is triggered with two conditions i.e. particle volume and distances. When the distance d between two pairwise particles satisfies $d \leqslant \sqrt{(2/3)V_0}$ which means the two merging particles are neighbors, and their volumes decrease to V_{min} (restriction on shrinkage of particle volume), the two particles would be merged into one particle with volume $2V_{min}$. Similar to particle splitting (Sun et al., 2021), the volume variation between before and after merging should also satisfy the relation as follows:

$$\| V_0 - V_{min} \| = \| 2V_{min} - V_0 \| \qquad (16)$$

Solving Eq. (16), $V_{min}=2/3V_0$ is obtained. The quantities of the merged particle (Sun et al., 2021) are assigned by following equations:
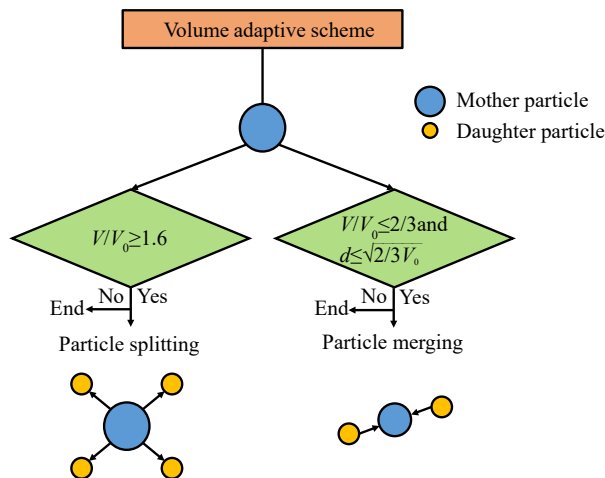

Figure 2 Sketch showing the volume adaptive scheme where V_0 represents the initial particle volume and d is the distance between two pairwise particles (Sun et al., 2021)

$$\begin{cases} \boldsymbol{r}_m = \frac{m_d^1 \boldsymbol{r}_d^1 + m_d^2 \boldsymbol{r}_d^2}{m_d^1 + m_d^1}; \quad \boldsymbol{v}_m = \frac{m_d^1 \boldsymbol{v}_d^1 + m_d^2 \boldsymbol{v}_d^2}{m_d^1 + m_d^2} \\ m_m = m_d^1 + m_d^2; \quad h_m = h_d; \quad V_m = \frac{m_m}{2\pi r_m \rho_m} \\ p_m = \frac{m_d^1 p_d^1 + m_d^2 p_d^2}{m_d^1 + m_d^2}; \quad \rho_m = F_{state}^{-1}(p_m), \end{cases} \qquad (17)$$

where the two daughter particles are denoted with the subscript d and superscripts 1 and 2, while the merging particle is denoted with the subscript m.

In the present axisymmetric SPH scheme, (see Eqs. (15) and (17)), since the fluid is assumed to be weakly-compressible, the smoothing lengths of all particles remain constant during the simulations, which helps to avoid the update of smoothing length and hence improves the computational efficiency.

In addition, in Sun et al. (2021b), the VAS is applied in the rising rubble problem, while in the present work, we co-opt and implement it to the water entry problems and correspondingly, the interaction between solid and fluid is supposed to be considered. Therefore, according to Newton's second law, the motion of moving rigid bodies in the vertical direction is obtained as follows

$$\frac{\mathrm{d}v^z}{\mathrm{d}t} = \frac{F^z}{M} - g^z,$$
$$F^z = \sum_{i \in \text{fluid}} \sum_{j \in \text{ghost}} - 2\pi r_i \, (p_i + p_j) \nabla_i W_{ij} V_i V_j, \qquad (18)$$

where M is the mass of moving bodies and the force F^z is calculated according to the balance between fluid particles (i) and ghost particles (j), see more details in the following section. Rotation is not considered in this work.

2.6 Boundary conditions

In the present work, the solid wall boundaries are discretized into ghost particles. The boundary-setting of water entry problems is plotted in Figure 3, taking the case of the water entry of the cone with $\beta = 20°$ as an example. The free-slip solid boundary is enforced on the solid wall. This is enforced by ignoring the viscous force between fluid and

Figure 3 Sketch for the numerical set up of the SPH simulations of the axisymmetric water entry problem (take the cone with deadrise angle of $\beta = 20°$ as an example)

ghost particles. Following Adami et al. (2012), the pressure of ghost particle p_g is extrapolated from the neighboring fluid particles to prevent boundary penetration. The formula is written as

$$p_g = \frac{\sum_f \left[p_f + \rho_f a_g \cdot (\boldsymbol{r}_f - \boldsymbol{r}_g) \right] W_{gf}}{\sum_f W_{gf}}, \qquad (19)$$

where the subscripts g and f denote the ghost particles and fluid particles, respectively. In addition, a sponge layer is implemented inside the stationary solid boundary to prevent pressure wave reflection. More details can be referred to Sun et al. (2015).

As for the treatment of multi-phases interface, an interface sharpness force F_i^s is introduced to the momentum equation to maintain the sharpness of the gas-water interface, see more details in Grenier et al. (2009). The compressibility of the air phase can be negligible when simulating the slamming stage of water entry problems (Yang and Qiu, 2012; Wang and Soares, 2020). But the air phase is supposed to be considered in the latter water entry process after the closing of the cavity, (see e.g. Wang and Soares (2020); Lyu et al. (2021)). But in the present work, we only focus on the slamming stage, so the air compressibility is not considered.

2.7 Computational cost

Implementing the axisymmetric SPH scheme, the 3D water entry problem can be simulated in two dimensions, which reduces the particle number and saves the computational cost effectively. Therefore, most simulations are finished in one day using 8 cores parallel computing on a desktop computer with Inter(R) Core(TM) i9-11900K CPU. However, for the cases with the highest particle resolution, $R/\Delta x = 400$ in this work, the time step becomes very small, the particle number reaches 4.5 million and therefore it takes several days to finish the SPH simulation. Even so, the particle number used in the axisymmetric SPH model is much reduced, which allows for the using of refined particle resolutions to capture the local pressure peak. In contrast, in purely 3D SPH simulations the computational costs would be much higher and capturing the local flow details is relatively difficult since the particle number in 3D would increase by several orders of magnitude.

3 Numerical results and discussions

3.1 Description of the axisymmetric water entry problem

In the current work, to extend the applicability of the axisymmetric SPH model to 3D axisymmetric water entry problems, following the experiment by De Backer et al. (2009),
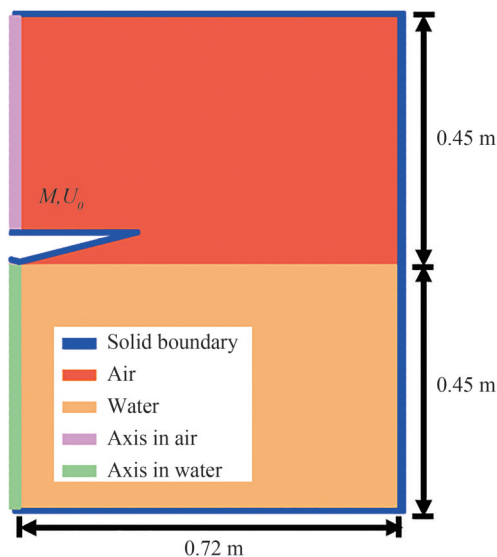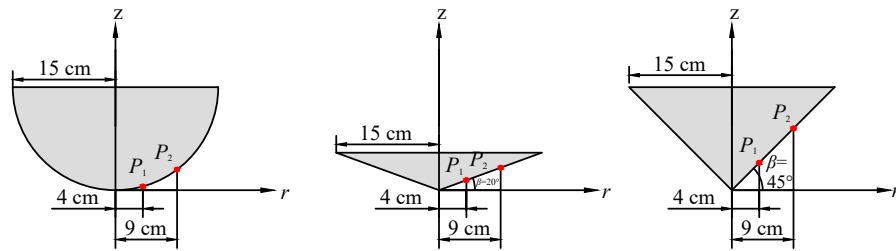
Figure 4 The sketch of the water entry bodies. Sphere (left) and cone with $\beta = 20°$ (middle) and $\beta = 45°$ (right) (De Backer et al., 2009). The length of body along the radial written as $R=0.15\ m$

water entries of a rigid sphere and two rigid cones with deadrise angles of 20° and 45° are selected. The parameters of mass and touch down velocity are listed in Table 1. Schematic diagrams of the sphere and cones are shown in Figure 4. The local pressure is probed at two locations signed as P_1 and P_2, represented by the coefficient C_P (Nair and Bhattacharyya, 2018), defined as:

$$C_P = \frac{P - P_0}{\frac{1}{2}\rho U_0^2}, \tag{20}$$

where P_0 and U_0 are the background pressure and touch-down velocity, respectively.

Table 1 Parameters of the water entry problems (Nair and Bhattacharyya, 2018)

Case	Radius R(m)	Mass M(kg)	Touch down velocity U_0 (m/s)
Sphere	0.15	11.5	4.0
Cone β=20°	0.15	9.8	3.85
Cone β=45°	0.15	10.2	4.05

3.2 Convergence analysis

In this section, a convergence analysis is performed based on the comparison of the pressure coefficients between SPH results of different particle resolutions as well as the experimental data (De Backer et al., 2009). For sphere water entry, four particle resolutions i.e. $R/\Delta x= 50$, $R/\Delta x= 100$,

$R/\Delta x= 200$ and $R/\Delta x= 400$ are adopted. The pressure coefficients C_P monitored at P_1 with four particle resolutions are plotted in Figure 5. In the initial particle distribution, the bottom of the sphere and water surface are apart as one particle spacing, i.e. Δx. That is to say, larger Δx means a little bit longer touch down distance so that a longer time is needed to reach the pressure peak. As plotted in Figure 5, with a finer particle resolution, the instant of pressure peak is closer to the one of experiment data (De Backer et al., 2009). With a rough particle resolution, the local high pressure peak is not resolved. At the finest particle resolution $R/\Delta x= 400$, the value of peak pressure is closest to the experimental data.
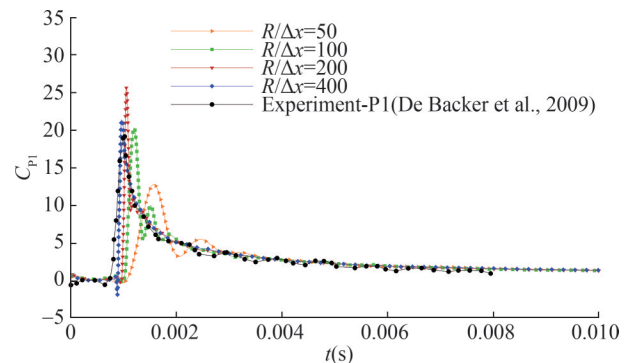

Figure 5 Time evolution of the impact pressure probed at location P_1 of sphere with four particle resolutions: SPH results are compared with experimental data (De Backer et al., 2009)
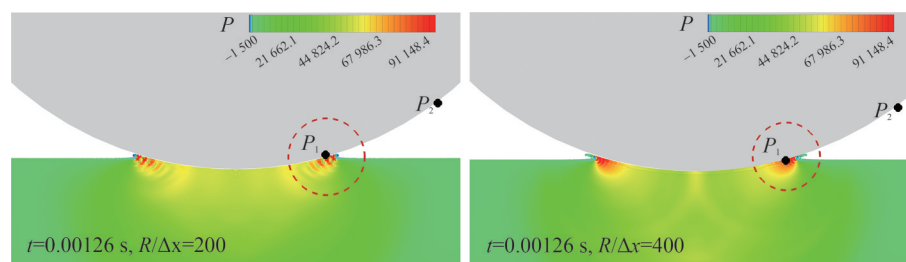

Figure 6 The pressure field when peak pressure propagates to the probing location P_1 for the sphere water entry simulated with particle resolutions $R/\Delta x = 200$ (left) and $R/\Delta x = 400$ (right)

To discuss the oscillating of the value of peak impact pressure at $R/\Delta x= 200$, the local pressure fields with particle resolutions $R/\Delta x= 200$ and $R/\Delta x= 400$ are compared in Figure 6. As one can observe, at the lower particle reso-
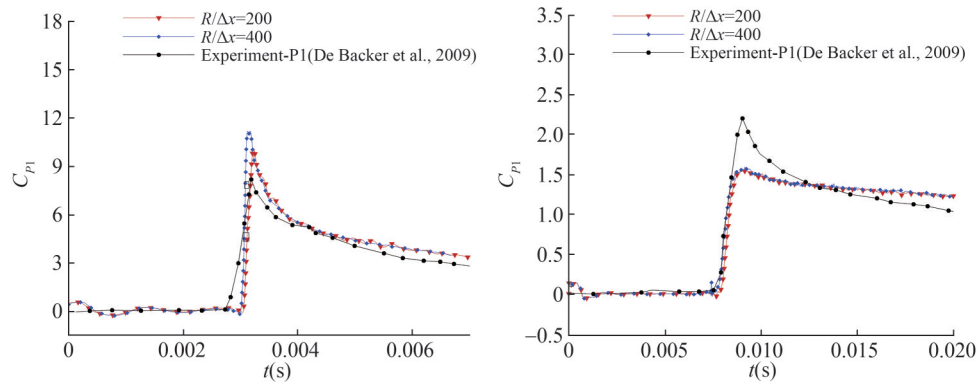
Figure 7 Time evolution of the impact pressure probed at location P_1 of cones with deadrise angle 20° (left) and 45° (right) with $R/\Delta x = 200$ and $R/\Delta x = 400$: SPH results are compared with experimental data (De Backer et al., 2009)

lution $R/\Delta x$= 200, the pressure field near the probing location P_1 encounters oscillations while with the refined one, i.e. $R/\Delta x$ =400, the pressure field becomes much smoother and shows less noise. The comparison implies that the uncertainty of peak pressure is tightly related to the particle resolution. The local oscillation of the pressure could lead to the changing of peak pressure since in SPH, the local pressure is measured on a single particle, while not the pressure averaged on the probe panel with an area larger than several particles. Comprehensive discussions on the uncertainty analysis of numerical simulations of slamming problems can be referred to Wang et al. (2021).

Thanks to the reduction of one dimension, the particle number used in axisymmetric SPH is less than that in 3D SPH simulations and therefore it is easier to refine particles to obtain better pressure field. In addition, in fully 3D SPH simulations, doubling the particle resolution will bring a particle number of eight times more, while with the present axisymmetric SPH scheme, doubling the particle resolution only increases the particle number to four times, which is much more efficient.

Based on the discussion above, the convergence study of the cases of two cones is directly simulate with particle spacing $R/\Delta x$= 200 and $R/\Delta x$= 400. As shown in Figure 7, time evolutions of the impact pressure are quite similar, indicating that for the cases of the cone's water entry, the particle resolutions $R/\Delta x$= 200 and $R/\Delta x$= 400 can be both applicable. Comparing the impact pressure of the sphere and cones, due to the smaller deadrise angle at the bottom of the sphere, the pressure peak is higher and sharper so that a higher particle resolution is needed. From above discussions, the water entry problem of the sphere is discussed in the following sections with the finest particle resolution $R/\Delta x$= 400 while for the cases with cones, the particle resolution $R/\Delta x$= 200 is used.

3.3 Water entry of a sphere

The water entry of a sphere is simulated, validated and discussed in this part. The mass of the sphere is M=11.5 kg and touchdown velocity is U_0=4.0 m/s as stated above.

The time histories of the impact pressure probed at two

different locations (P_1 and P_2) are also plotted in Figure 8 where the SPH result is compared with experimental data (De Backer et al., 2009) and other numerical results obtained via FVM (Nair and Bhattacharyya, 2018). As one can see, the tendency of the pressure evolutions agrees well between the numerical results and the experiment data (De Backer et al., 2009), but a little discrepancy for the pressure peaks is also observed. Generally, the numerical monitors are more sensitive to transient variation of pressure comparing with the experimental sensors. This is because, in experiments, pressure is measured by averaging pressure over the area of the sensor panel while in the SPH simulations, pressure can be captured on a single particle which is much smaller than the sensor panel, which can, therefore, cause a higher pressure peak for the cases of smaller deadrise angle, i.e. the water entries of sphere and cone with smaller deadrise angle, e.g. β= 20°. A similar analysis was also conducted by Wang et al. (2015). Observing the result at location P_2, the SPH result has a better agreement with the FVM result (Nair and Bhattacharyya, 2018) including the rising time and peak values. In addition, to further validate the accuracy of the SPH results, the vertical motion of the sphere, including the impact velocity and penetration depth, is compared with reference results, see Figure 9. The impact velocity is similar to the experimental data (De Backer et al., 2009)
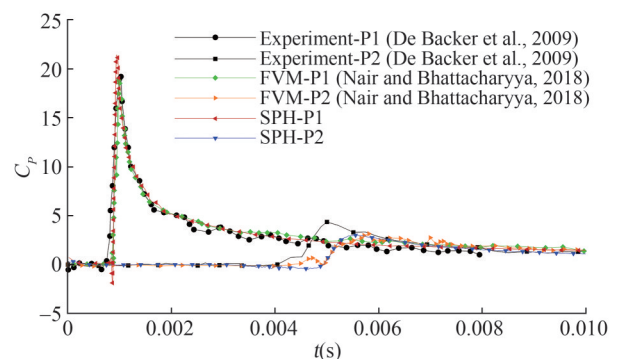

Figure 8 Pressure probed at two locations P_1 and P_2: SPH results compared with experimental data (De Backer et al., 2009) and FVM results (Nair and Bhattacharyya, 2018)

(a) Time evolution of impact velocity

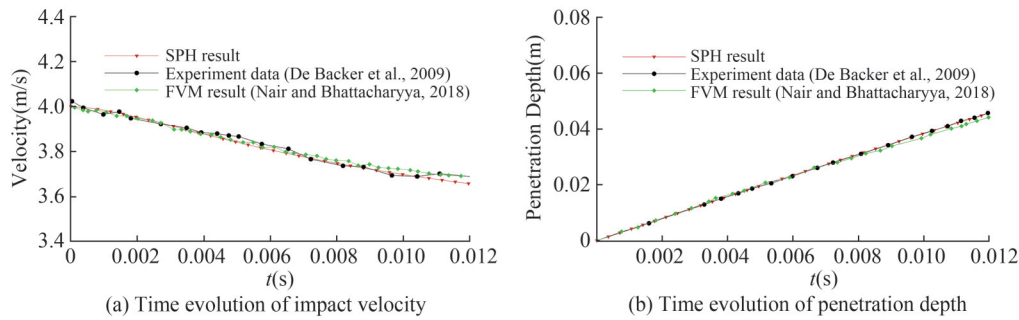(b) Time evolution of penetration depth

Figure 9 Vertical motion of water entry of sphere: SPH results compared with experimental data (De Backer et al., 2009) and FVM results (Nair and Bhattacharyya, 2018)

and numerical result (Nair and Bhattacharyya, 2018). Moreover, with time gone by, the SPH result is closer to the experimental data compared to the FVM result. Probing the penetration depth, a good agreement is achieved between SPH results and both reference results.

The snapshots during the water entry process are displayed in Figure 10. We note that the air particles are blanked to better visualize the water surface and splashing jets. It can be observed that the qualitative comparison between the experiment (De Backer et al., 2009) and SPH also shows good agreement. Further, the splashing of water jets can be accurately captured. In general, the axisymmetric SPH results are fairly satisfactory.

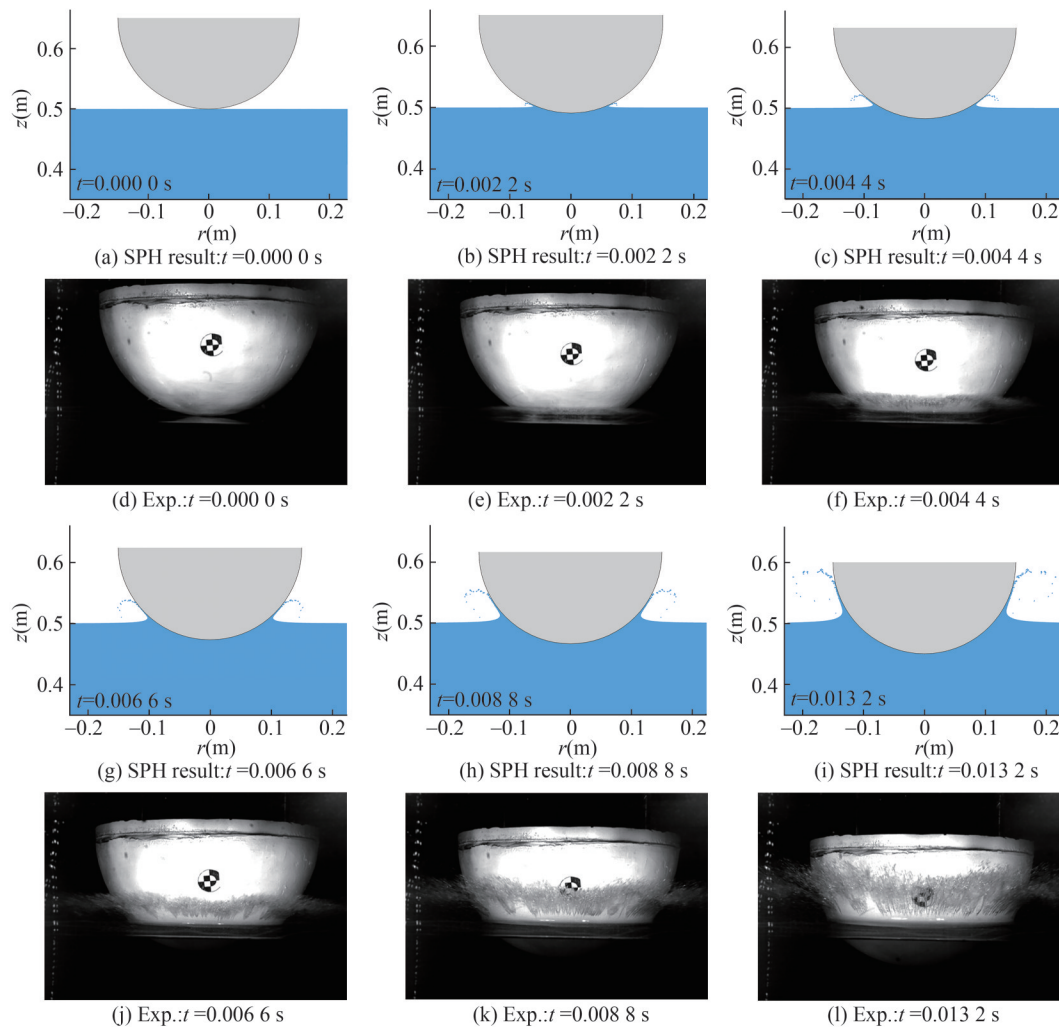Figure 11 displays the pressure field around the sphere at

(a) SPH result:t =0.000 0 s

(b) SPH result:t =0.002 2 s

(c) SPH result:t =0.004 4 s

(d) Exp.:t =0.000 0 s

(e) Exp.:t =0.002 2 s

(f) Exp.:t =0.004 4 s

(g) SPH result:t =0.006 6 s

(h) SPH result:t =0.008 8 s

(i) SPH result:t =0.013 2 s

(j) Exp.:t =0.006 6 s

(k) Exp.:t =0.008 8 s

(l) Exp.:t =0.013 2 s

Figure 10 Comparison between the present axisymmetric SPH results and the experimental snapshots in De Backer et al. (2009) for the water entry of a sphere
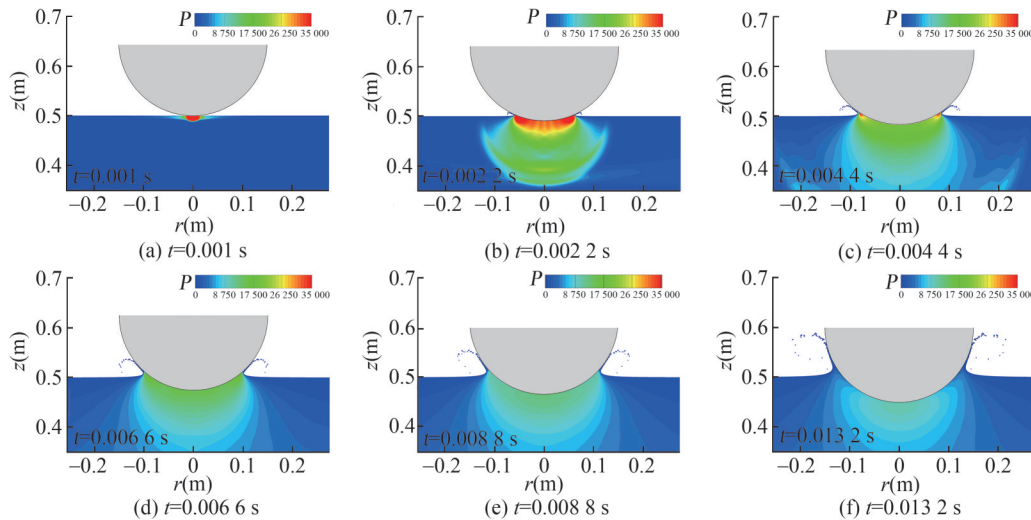
Figure 11   The pressure fields at several time instants for the water entry problem of sphere

different time instants. It is demonstrated that the present axisymmetric SPH model is able to provide a smooth pressure field, which is very important for estimating the slamming loads in ocean engineering.

3.4 Water entry of a cone with β = 20°

In this part, the water entry problem of a cone with deadrise angle of 20° is simulated and discussed. Figure 12 shows the time evolutions of the impact pressure measured at locations P_1 and P_2. The comparison is made between SPH simulations, experimental data (De Backer et al., 2009) and FVM results (Nair and Bhattacharyya, 2018). As one can observe, the numerical result of C_P probed in P_2 agrees well with the reference solution. At P_1, the trend of the pressure coefficient of three methods resembles each other, while the pressure peak value of SPH result is a little larger than the other two. However, C_P probed at P_1 after the peak and the C_P probed at P_2 are both closer to experiment data compared with the FVM results. The discrepancy of pressure peak at P_1 can be caused by the uncertainty of the pressure probe when measuring the slamming pressure at a small deadrise angle near the bottom of the cone. As shown in Wang et al. (2015), repeated experiments show a large deviation (error bars) at the instant of peak pressure. Further, the weakly-compressible assumption (the pressure is linked to the density linearly) in the present SPH scheme may also lead to the difference of the numerical results.

Figure 13 shows the vertical velocity and penetration depth compared with reference results. As it is plotted, the penetration depth shows good agreement with experimental data and FVM results. As for the velocity, the SPH result shows good agreement with only slight difference appearing at the latter stage. Figure 14 shows the comparison of the snapshots between SPH and experiment (De Backer et al.,

Figure 12   Pressure probed at two locations P_1 and P_2 of cone with deadrise angle of β=20°, compared with experimental data in De Backer et al. (2009) and results of Nair and Bhattacharyya (2018) using FVM, respectively
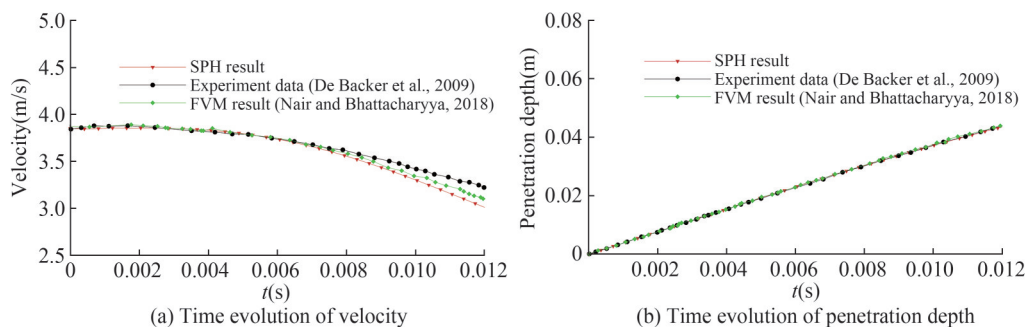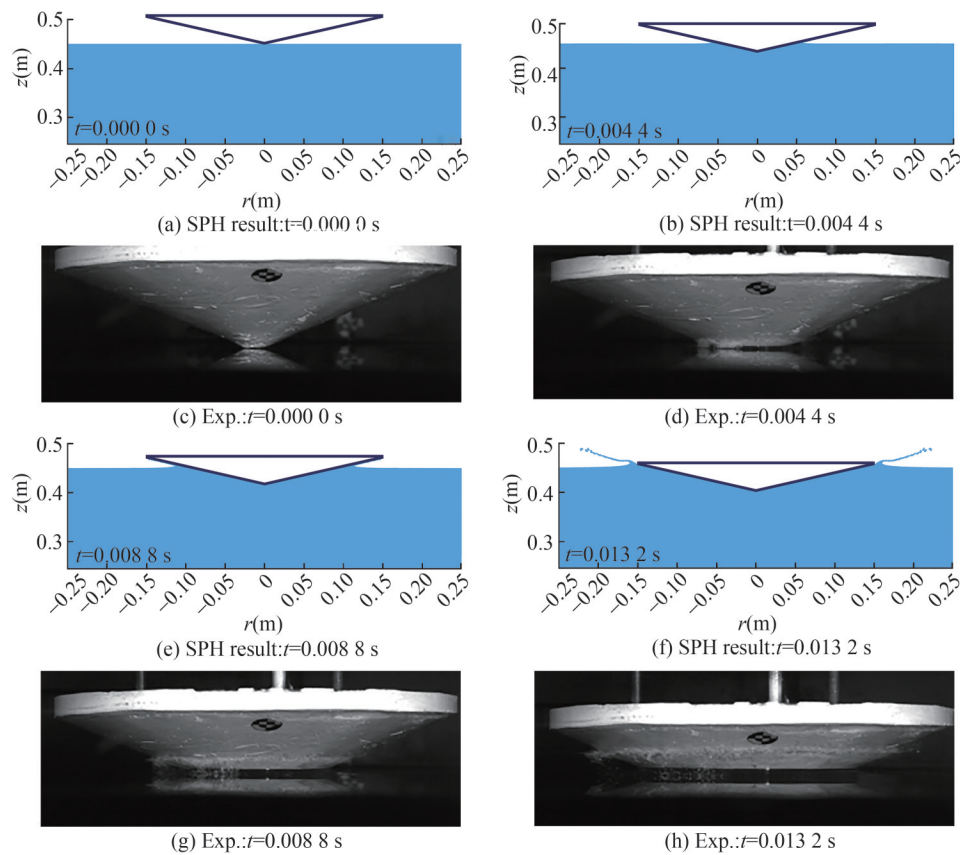

(a) Time evolution of velocity

(b) Time evolution of penetration depth

Figure 13   Vertical motion of water entry of the cone with deadrise angle β=20°

Figure 14 Results of the water entry problem of a cone with deadrise angle of $\beta=20°$. Comparison between the present axisymmetric SPH results and the experimental snapshots in De Backer et al. (2009)
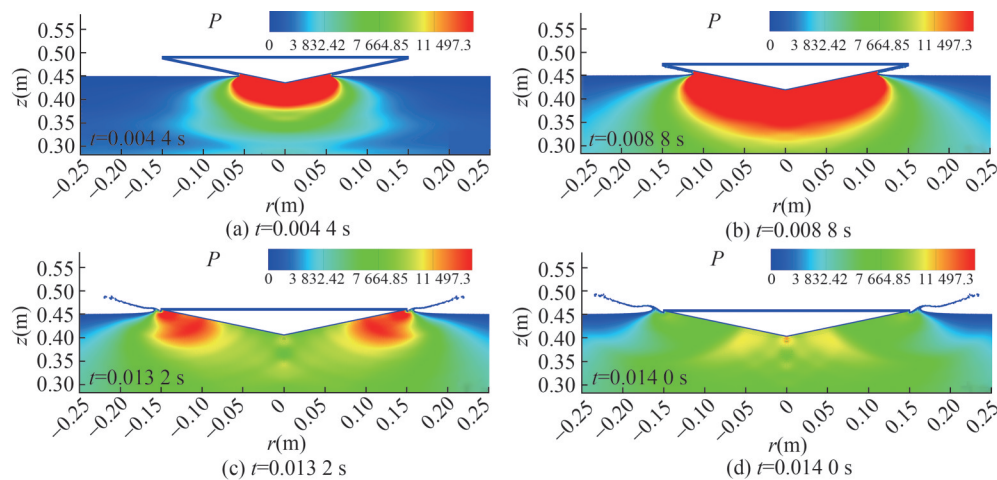

Figure 15 The pressure fields at several time instants for the water entry problem of the cone with $\beta=20°$

2009). Observing the free surface deformation, the water splashing can be well captured in SPH, which could be challenging for grid-based methods. Therefore, it is demonstrated that the axisymmetric SPH model is able to accurately simulate the water entry problem of a cone with a small deadrise angle of 20°. Figure 15 depicts the pressure field around the cone. As one can see, a smooth pressure field is obtained again and the maximum pressure is located near the intersec-

tions between the cone surface and the free-surface.

3.5 Water entry of a cone with $\beta = 45°$

In this part, a cone with deadrise angle of 45° entering undisturbed water is simulated. The time evolution of impact pressure monitored at the two locations P_1 and P_2 is shown in Figure 16. The time instant of pressure rise is accurately
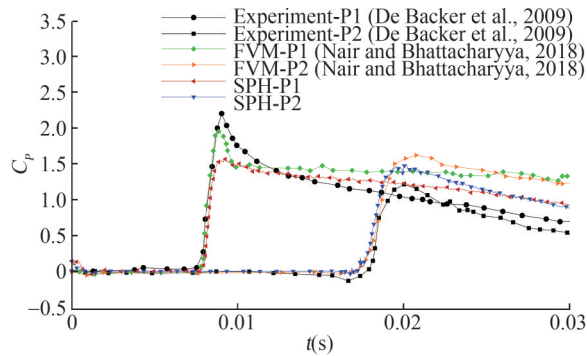
Figure 16 Pressure probed at two locations P_1 and P_2 of cone with deadrise angle of $\beta=45°$, compared with experimental data in De Backer et al. (2009) and results of Nair and Bhattacharyya (2018) using FVM respectively

predicted by both SPH and FVM solvers (Nair and Bhattacharyya, 2018), while lower pressure peak is predicted at location P_1 and a larger pressure peak is predicted at P_2. As discussed by Iafrati et al. (2015), the local pressure measured in experiments is very sensitive and can be affected by many uncertainties, which is related to the probes and their installation. As also discussed by Wang et al. (2015), by repeating the same water entry experiment, the error bar of the peak pressure was not negligible. There are many uncertainties that could affect the exact peak value of pressure. Therefore,
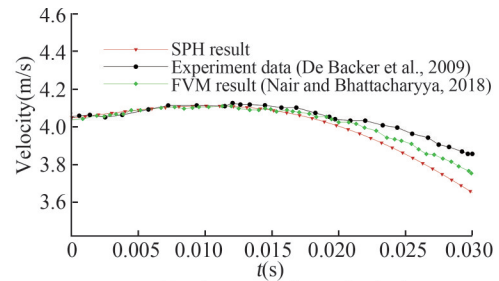
(a) Time evolutions of velocity
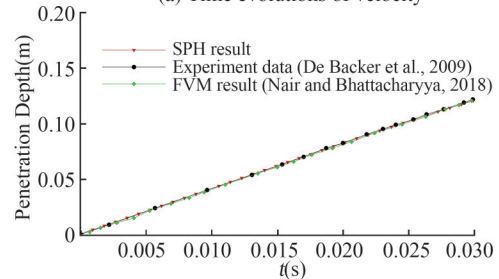
(b) Time evolution of penetration depth

Figure 17 Vertical motion of water entry of the cone with deadrise angle $\beta=45°$

for cone with deadrise angle of $\beta=45°$, the reason why the pressure peak at P1 is underestimated is still an open problem. However, at P_2, the SPH result is obviously closer to the experimental data. In addition, comparing the peak values
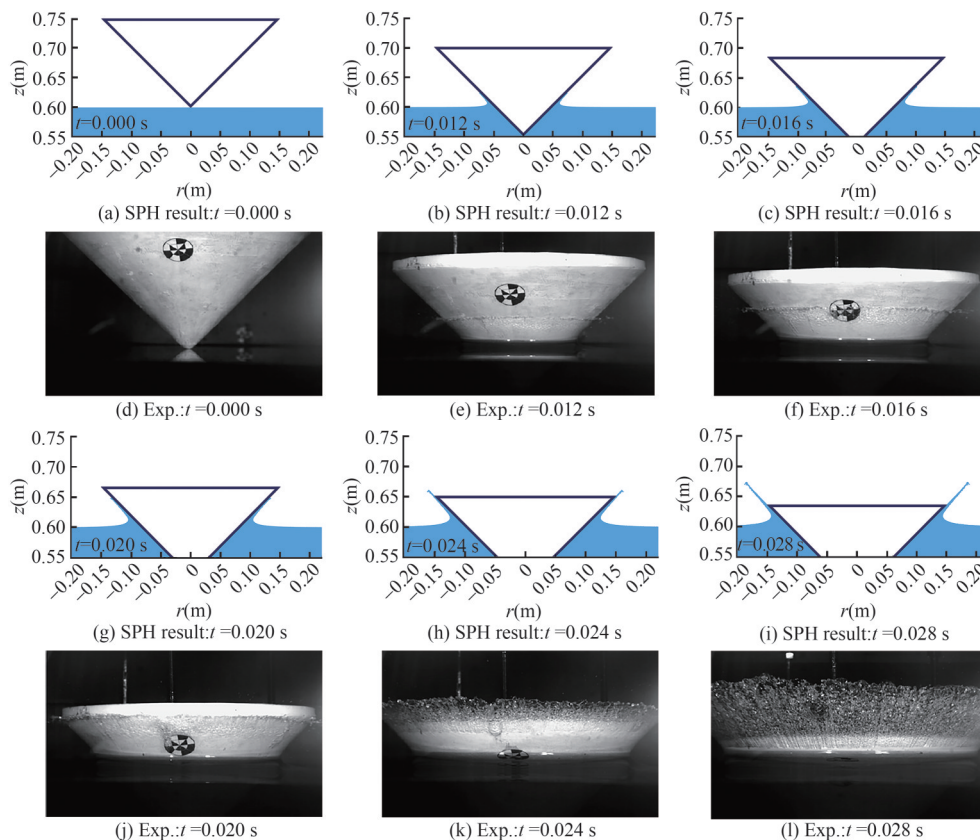

(a) SPH result:t =0.000 s

(b) SPH result:t =0.012 s

(c) SPH result:t =0.016 s

(d) Exp.:t =0.000 s

(e) Exp.:t =0.012 s

(f) Exp.:t =0.016 s

(g) SPH result:t =0.020 s

(h) SPH result:t =0.024 s

(i) SPH result:t =0.028 s

(j) Exp.:t =0.020 s

(k) Exp.:t =0.024 s

(l) Exp.:t =0.028 s

Figure 18 Results of the water entry problem of a cone with deadrise angle of $\beta=45°$. Comparison between the axisymmetric SPH results and the experimental snapshots in De Backer et al. (2009)
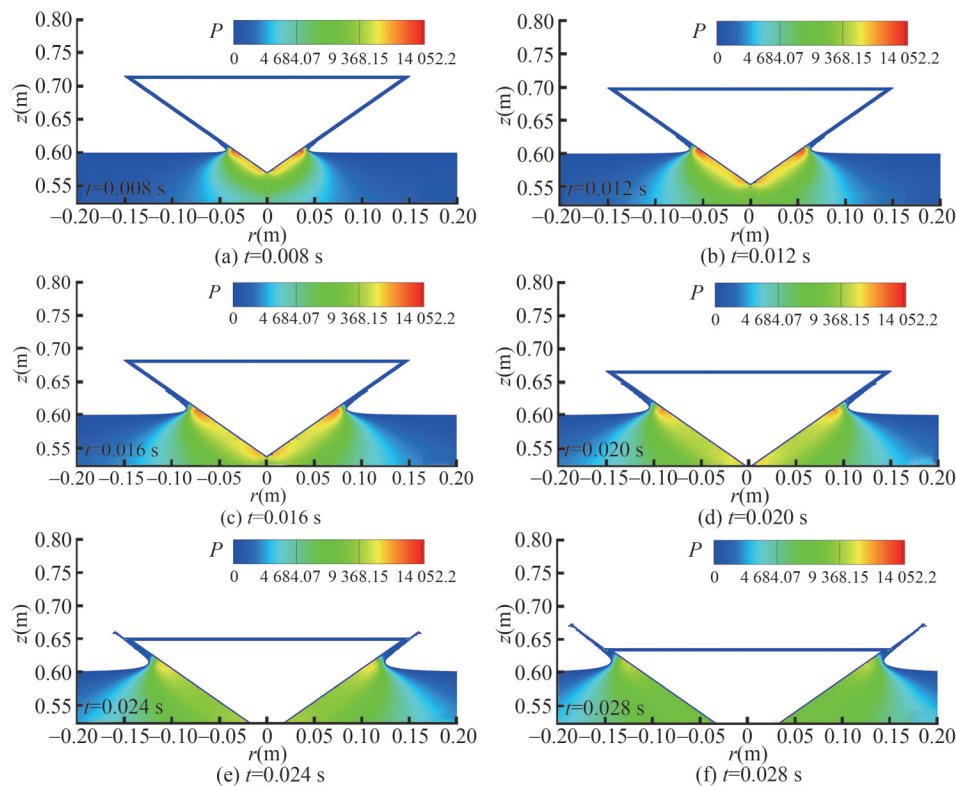
Figure 19 The pressure fields at several time instants for the water entry problem of the cone with $\beta=45°$

of C_P between cases with deadrise angles of 20° and 45°, the C_P of $\beta = 20°$ is significantly larger than the one of $\beta = 45°$, confirming that the deadrise angle plays an important role in the slamming load. It can also be observed qualitatively that, for the case with a larger deadrise angle of $\beta =45°$, the lasting time of the high pressure is longer and the pressure variation is slower than the simulation for the cone with deadrise angle of $\beta =20°$. The comparison of the cone's vertical motion is shown in Figure 17. An accurate match is presented in the initial stage while the difference starts to appear after the first pressure peak. This result is also reported in Nair and Bhattacharyya (2018) and Wang and Soares (2014). Different to the velocity curves, the penetration depth can be accurately predicted and a good agreement is obtained between SPH and reference results.

Figure 18 shows the comparison between the SPH and experimental snapshots (De Backer et al., 2009). Obviously, the qualitative comparison presents a good agreement. Further, the pressure field can be well predicted without noise, as shown in Figure 19.

4 Conclusions and perspectives

In this work, an axisymmetric SPH model is applied to solve different axisymmetric water entry problems, including water entry of spheres and cones with different deadrise angles. Based on the comparisons between SPH results and experimental data, the axisymmetric SPH model is shown to be accurate, reliable and efficient for such kind of water entry problems. The local impact pressure of a moving body with a small deadrise is predicted well with refined particle resolutions, which is challenging in terms of the computational cost for fully three dimensional SPH simulations, while the axisymmetric SPH model can sufficiently improve computational efficiency and achieves high numerical accuracy. In addition, the splashing jets are successfully captured with the two-phase SPH scheme and agree fairly well with the experimental snapshots.

In future studies, the present axisymmetric SPH model will be further extended for solving water entry problems with higher speeds, studying the impact pressure considering the fluid compressibility effects. The compression of the gas cavity entrapped during water entry should be considered to study the water entry dynamics after pinch-off (see e. g. the 2D study in Lyu et al. (2021)). In addition, the present axisymmetric SPH scheme is limited to the water entry problems of axisymmetric bodies. The 3D SPH simulation for water entry of marine structures with complex shapes is also necessary to be developed and the numerical efficiency can be improved with the implementation of Adaptive Particle Refinement (APR) (Chiron et al., 2018) and GPU parallel computing (Lyu et al., 2022b).

References

Adami S, Hu XY and Adams NA (2012) A generalized wall boundary condition for smoothed particle hydrodynamics. Journal of Computational Physics 231(21): 7057-7075

Antuono M, Colagrossi A and Marrone S (2012) 12. Numerical diffusive terms in weakly-compressible SPH schemes. Computer Physics Communications 183: 2570-2580. https://doi.org/10.1016/j.cpc.2012.07.006

Antuono M, Colagrossi A, Marrone S and Molteni D (2010) Free-surface ows solved by means of SPH schemes with numerical diusive terms. Computer Physics Communications 181(3): 532-549. https: //doi.org/10.1016/j.cpc.2009.11.002

Aristo JM, Truscott TT, Techet AH and Bush JWM (2010) The water entry of decelerating spheres. Physics of Fluids 22(3): 032102. https:// doi.org/10.1063/1.3309454. https://doi.org/10.1063/ 1.3309454

Bckmann A, Shipilova O and Skeie G (2012) Incompressible SPH for free surface ows. Computers & Fluids 67: 138-151

Brookshaw L (2003) April. Smooth particle hydrodynamics in cylindrical coordinates. In K. Burrage and R. B. Sidje (Eds.), Proc. of 10th Computa- tional Techniques and Applications Conference CTAC-2001, Volume 44: pp. C114-C139

Cheng H, Ming F, Sun P, Sui Y and Zhang AM (2020) Ship hull slamming analysis with smoothed particle hydrodynamics method. Applied Ocean Research 101: 102268. https://doi.org/10.1016/j.apor.2020.102268

Chiron L, Oger G, De Lee M and Touze DL (2018) Analysis and im-provements of adaptive particle renement (APR) through cpu time, accuracy and robustness considerations. Journal of Computational Physics 354: 552-575. https://doi.org/10.1016/j.jcp.2017.10.041

Colagrossi A and Landrini M (2003) Numerical simulation of interfa-cial ows by smoothed particle hydrodynamics. Journal of Computa- tional Physics 191(2): 448-475. https://doi.org/10.1016/ S0021-9991 (03)00324-3

De Backer G, Vantorre M, Beels C, De Pre J, Victor S, De Rouck J, Blommaert C and Van Paepegem W (2009) Experimental investigation of water impact on axisymmetric bodies. Applied Ocean Research 31(3): 143-156. https://doi.org/10.1016/j.apor.2009.07.003

Dobrovol'skaya ZN (1969) On some problems of similarity ow of uid with a free surface. Journal of Fluid Mechanics 36(4): 805-829. https://doi.org/ 10.1017/S0022112069001996

Fang XL, Colagrossi A, Wang PP and Zhang AM (2022) An accu-rate and robust axisymmetric SPH method based on riemann solver with applications in ocean engineering. Ocean Engineer-ing 244: 110369. https: //doi.org/10.1016/j.oceaneng.2021.110369

Gong K, Shao S, Liu H, Lin P and Gui Q (2019) Cylindrical smoothed particle hydrodynamics simulations of water entry. Journal of Fluids Engineering 141: 7

Gong K, Shao S, Liu H, Wang B and Tan SK (2016) Two-phase SPH simulation of uid-structure interactions. Journal of Fluids and Struc-tures 65: 155-179. https://doi.org/10.1016/j.j uidstructs. 2016.05.012

Grenier N, Antuono M, Colagrossi A, Le Touze D and Alessandrini B (2009) An hamiltonian interface SPH formulation for multi-uid and free surface ows. Journal of Computational Physics 228

(22): 8380-8393

Hammani I, Marrone S, Colagrossi A, Oger G and Le Touze D (2020) Detailed study on the extension of the -SPH model to multi-phase ow. Computer Methods in Applied Mechanics and Engineering 368: 113189

He F, Zhang H, Huang C and Liu M (2020) Numerical investigation of the solitary wave breaking over a slope by using the nite particle method. Coastal Engineering 156: 103617. https://doi.org/10.1016/ j.coastaleng.2019.103617

He F, Zhang H, Huang C and Liu M (2022) A stable SPH model with large c numbers for multi-phase ows with large density ratios. Journal of Computational Physics: 110944

Huang L, Tavakoli S, Li M, Dolatshah A, Pena B, Ding B and Dashtimanesh A(2021) Cfd analyses on the water entry process of a freefall lifeboat. Ocean Engineering 232: 109115. https://doi.org/10.1016/j. oceaneng.2021.109115

Iafrati A, Grizzi S, Siemann M and Monta~nes LB (2015) High-speed ditching of a at plate: Experimental data and uncertainty assessment. Journal of Fluids and Structures 55: 501-525

Iranmanesh A and Passandideh-Fard M (2017) A three-dimensional numerical approach on water entry of a horizontal circular cylinder using the volume of uid technique. Ocean Engineering 130: 557-566. https://doi.org/https: //doi.org/10.1016/j.oceaneng.2016.12.018

Khayyer A and Gotoh H (2016) A multiphase compressible-incom-pressible particle method for water slamming. International Jour-nal of Oshore and Polar Engineering 26(01): 20-25

Lin MC and Shieh LD (1997) Simultaneous measurements of water impact on a two-dimensional body. Fluid Dynamics Research 19(3): 125

Lin P (2007) A xed-grid model for simulation of a moving body in free surface ows. Computers & Fluids 36(3): 549-561. https: //doi.org/10.1016/j.comp uid.2006.03.004

Liu M and Zhang Z (2019) Smoothed particle hydrodynamics (SPH) for modeling uid-structure interactions. SCIENCE CHINA Physics, Mechanics & Astronomy62 (8): 984701

Long T, Zhang Z and Liu M (2021) Multi-resolution technique integrated with smoothed particle element method (spem) for modeling uid-structure interaction problems with free surfaces. Science China Physics, Mechanics & Astronomy 64(8): 1-22

Luo M, Khayyer A and Lin P (2021) Particle methods in ocean and coastal engineering. Applied Ocean Research 114: 102734

Lyu HG, Deng R, Sun PN and Miao JM (2021) Study on the wedge penetrating uid interfaces characterized by dierent density-ratios: Numerical investigations with a multi-phase SPH model. Ocean Engineering 237: 109538. https://doi.org/10.1016/j. oceaneng. 2021.109538

Lyu HG, Sun PN, Huang XT, Zhong SY, Peng YX, Jiang T and Ji CN (2022a) A review of SPH techniques for hydrodynamic simulations of ocean energy devices. Energies 15(2): 502

Marrone S, Colagrossi A, Park J and Campana E (2017) Challenges on the numerical prediction of slamming loads on lng tank insulation panels. Ocean Engineering 141: 512-530. https://doi.org/10.1016/ j.oceaneng.2017.06.041

Ming Fr, Sun PN, Zhang AM, et al (2014) Investigation on charge parameters of underwater contact explosion based on axisymmetric SPH method. Applied Mathematics and Mechanics 35(4): 453-468

Moghisi M and Squire P (1981) 07. An experimental investigation of the initial force of impact on a sphere striking a liquid surface. Journal of Fluid Mechanics 108: 133-146. https://doi.org/10.1017/ S0022112081002036

Nair VV and Bhattacharyya S (2018) Water entry and exit of axisymmetric bodies by cfd approach. Journal of Ocean Engineering and Science 3(2): 156-174. https://doi.org/10.1016/j.joes.2018. 05.002

Oger G, Doring M, Alessandrini B and Ferrant P (2006) Two-dimensional SPH simulations of wedge water entries. Journal of Computational Physics 213(2): 803-822. https://doi.org/10.1016/j.jcp. 2005.09.004

Omidvar P, Stansby PK and Rogers BD (2012) Wave body interaction in 2d using smoothed particle hydrodynamics (SPH) with variable particle mass. International Journal for Numerical Methods in Fluids 68(6): 686-705

Randles P and Libersky LD (1996) Smoothed particle hydrodynamics: some recent improvements and applications. Computer methods in applied mechanics and engineering 139(1-4): 375-408

Shao S (2009) Incompressible SPH simulation of water entry of a free-falling object. International Journal for Numerical Methods in Fluids 59(1): 91-115. https://doi. org/10.1002/d.1813.

Shao S and Gotoh H (2004) Simulating coupled motion of progressive wave and oating curtain wall by SPH-les model. Coastal Engineering Jour- nal 46(2): 171-202. https://doi.org/10.1142/S0578563404001026.

Skillen A, Lind S, Stansby PK and Rogers BD (2013a) Incompressible smoothed particle hydrodynamics (SPH) with reduced temporal noise and generalised ckian smoothing applied to body-water slam and ecient wave-body interaction. Computer Methods in Applied Mechanics and Engi- neering 265: 163-173. https://doi.org/10.1016/j.cma.2013. 05.017

Skillen A, Lind S, Stansby PK and Rogers BD (2013b) Incompressible smoothed particle hydrodynamics (SPH) with reduced temporal noise and generalised ckian smoothing applied to body-water slam and ecient wave-body interaction. Computer Methods in Applied Mechanics and Engi- neering 265: 163-173. https://doi.org/10.1016/j.cma.2013. 05.017

Sun P, Colagrossi A, Marrone S, Antuono M and Zhang AM (2019) A consistent approach to particle shifting in the-plus-SPH model. Computer Methods in Applied Mechanics and Engineering 348: 912-934

Sun P, Colagrossi A, Marrone S and Zhang A (2017) The plus-SPH model: Simple procedures for a further improvement of the SPH scheme. Computer Methods in Applied Mechanics and Engineering 315: 25-49. https://doi.org/10.1016/j.cma.2016.10.028

Sun P, Colagrossi A, Touze DL and Zhang AM (2019) Extension of the-plus-SPH model for simulating vortex-induced-vibration problems. Jour-nal of Fluids and Structures 90: 19-42. https://doi.org/10. 1016/j.j uidstructs.2019.06.004

Sun P, Ming F and Zhang A (2015) Numerical simulation of interactions between free surface and rigid body using a robust SPH method. Ocean Engineering 98: 32-49

Sun P, Zhang AM, Marrone S and Ming F (2018) An accurate and e-cient SPH modeling of the water entry of circular cylinders. Applied Ocean Research 72: 60-75. https://doi.org/10.1016/j. apor.2018. 01.004

Sun PN, Le Touze D, Oger G and Zhang AM (2021a) An accurate fsi-SPH modeling of challenging uid-structure interaction problems in two and three dimensions. Ocean Engineering 221: 108552

Sun PN, Le Touze D, Oger G and Zhang AM (2021b) An accurate SPH volume adaptive scheme for modeling strongly-compressible multiphase ows. part 2: Extension of the scheme to cylindrical coordinates and simulations of 3d axisymmetric problems with experimental validations. Journal of Computational Physics 426: 109936

Sun PN, Le Touze D, Oger G and Zhang AM (2021) An accurate SPH volume adaptive scheme for modeling strongly-compressible multiphase ows. part 1: Numerical scheme and validations with basic 1d and 2d benchmarks. Journal of Computational Physics 426: 109937. https://doi.org/10.1016/j.jcp.2020.109937

Truscott TT and Techet AH (2009) Water entry of spinning spheres.

Journal of Fluid Mechanics 625: 135-165

Van Nuel D, Vepa K, De Baere I, Lava P, Kersemans M, Degrieck J, De Rouck J and Van Paepegem W (2014) A comparison between the experimental and theoretical impact pressures acting on a horizontal quasirigid cylinder during vertical water entry. Ocean Engineering 77: 42-54. https://doi.org/10.1016/j.oceaneng.2013.11.019

Vandamme J, Zou Q and Reeve DE (2011) Modeling oating object entry and exit using smoothed particle hydrodynamics. Journal of Waterway, Port, Coastal, and Ocean Engineering 137(5): 213-224

Von Karman T and Wattendorf F (1929) The impact of sea planes during landing. naca tech. Technical report, Note 321

Wagner H (1932) Phenomena associated with impacts and sliding on liquid surfaces. Journal of Applied Mathematics and Mechanics 12(4): 193-215

Wang J, Lugni C and Faltinsen OM (2015) Experimental and numerical investigation of a freefall wedge vertically entering the water surface. Applied Ocean Research 51: 181-203

Wang L, Xu F and Yang Y (2019) SPH scheme for simulating the water entry of an elastomer. Ocean Engineering 178: 233-245

Wang S, Islam H and Soares CG (2021) Uncertainty due to discretization on the ale algorithm for predicting water slamming loads. Marine Structures 80: 103086

Wang S and Soares CG (2014) Numerical study on the water impact of 3d bodies by an explicit nite element method. Ocean Engineering 78: 73-88

Wang S and Soares CG (2020) Eects of compressibility, threedimensionality and air cavity on a free-falling wedge cylinder. Ocean Engineering 217: 107589

Wang S. and Soares CG (2022) Three-dimensional eects on slamming loads on a free-falling bow- are cylinder into calm water. Journal of Oshore Mechanics and Arctic Engineering 144(4): 044502

Wang S, Xiang G and Soares CG (2021) Assessment of three-dimensional eects on slamming load predictions using openfoam. Applied Ocean Research 112: 102646

Woodgate MA, Barakos GN, Scrase N and Neville T (2019) Simulation of helicopter ditching using smoothed particle hydrodynamics. Aerospace Science and Technology 85: 277-292. https://doi.org/10. 1016/j.ast.2018.12.016

Xiao T, Qin N, Lu Z, Sun X, Tong M and Wang Z (2017) Development of a smoothed particle hydrodynamics method and its application to aircraft ditching simulations. Aerospace Science and Technology 66: 28-43. https://doi.org/10.1016/j.ast.2017.02.022

Yang Q and Qiu W (2012) Numerical simulation of water impact for 2d and 3d bodies. Ocean Engineering 43: 82-89

Yang Q, Xu F, Yang Y and Wang L (2020) A multi-phase SPH model based on riemann solvers for simulation of jet breakup. Engineering Analysis with Boundary Elements 111: 134-147

Ye T, Pan D, Huang C and Liu M (2019) Smoothed particle hydrodynamics (SPH) for complex uid ows: Recent developments in methodology and applications. Physics of Fluids 31(1): 011301. https://doi.org/10.1063/1.5068697

Yettou EM, Desrochers A and Champoux Y (2006) Experimental study on the water impact of a symmetrical wedge. Fluid Dynamics Research 38 (1): 47

Yu J, Liu Z, Zhang X and Zhang H (2015) CFD numerical simulation of air-liquid two-phase ow in vertical tube of airlift pump. Water Resources and Hydropower Engineering 46(9): 144-147

Zhang AM, Sun PN, Ming FR and Colagrossi A (2017) Smoothed particle hydrodynamics and its applications in fluid-structure interactions. Journal of Hydrodynamics, Ser. B 29(2): 187-216

Zhao R and Faltinsen O (1993) Water entry of two-dimensional bodies. Journal of uid mechanics 246: 593-612